processes

MDPI

Article

Robust Design and Operation of a Multistage Reactor for Methanol Synthesis from Renewable Resources

Tobias Keßler [1,*] and Achim Kienle [1,2,*]

[1] Chair for Automation/Modelling, Otto von Guericke University Magdeburg, Universitätsplatz 2, 39106 Magdeburg, Germany
[2] Process Synthesis and Process Dynamics, Max Planck Institute for Dynamics of Complex Technical Systems, Sandtorstraße 1, 39106 Magdeburg, Germany
* Correspondence: tobias.kessler@ovgu.de (T.K.); achim.kienle@ovgu.de (A.K.)

Abstract: Methanol is an important raw material widely used in the chemical industry. This article addresses the challenge of fluctuations in green hydrogen as a feed stream for methanol production from renewable feedstock. For a staged reactor design, robust operating conditions are generated through the simultaneous steady-state optimization of 50 process scenarios. The feed can be split and fed separately to the different reactor stages. However, neglected transient effects may render this design infeasible under dynamic conditions concerning carbon conversion and reactor temperature constraints. To overcome this, an additional dynamic optimization is conducted to ensure a feasible operation by an optimized feed-forward control of feed distribution and shell temperatures. In practice, this is possible because the disturbance, i.e., fluctuation, is measurable and predictable in a short time frame. The optimization yields optimal operating conditions, resulting in a reactor that is dynamically feasible for measurable fluctuating inlet conditions.

Keywords: robust optimization; dynamic optimization; methanol synthesis; renewable resources; julia

Citation: Keßler, T.; Kienle, A. Robust Design and Operation of a Multistage Reactor for Methanol Synthesis from Renewable Resources. *Processes* **2023**, *11*, 2928. https://doi.org/10.3390/pr11102928

Academic Editors: Stefania Tronci, Massimiliano Errico, Riccardo Bacci Di Capaci, Ingmar Nopens, Elena Torfs and Michael Short

Received: 21 August 2023
Revised: 22 September 2023
Accepted: 29 September 2023
Published: 7 October 2023

1. Introduction

Methanol is a widely used and important raw material for the chemical industry [1,2]. It can also be used for chemical energy storage [1,3]. Today, methanol is produced large-scale using fossil-based synthesis gas in heterogeneously catalyzed reactions. The world-wide annual production is 98 million tonnes [4]. Of that, only a small fraction, i.e., 0.2 million tonnes, is produced from renewable resources [4]. In the light of climate change, it becomes clear that green methanol will play an important role [5,6]. For the production of green methanol, the fossil-based raw materials need to be substituted by renewables. Possible carbon sources are, among others, biogas [7,8], industrial fumes [9], and direct CO_2 air capture [10]. A suitable hydrogen source is electrolysis using electricity produced by solar, wind, or water power [8,11]. Due to the transformation of the energy supply system, there are already a number of pilot-scale plants for the production of green methanol in operation [12]. However, as of today, the costs for renewable methanol are still much higher than for its fossil counterpart. This might change in the future due to legislation or more efficient processes [11,13,14].

One of the challenges in the production of green methanol is to cope with fluctuations in the feed streams [15–17], e.g., a varying availability of regenerative electricity and hence hydrogen. Conventional processes are operated under steady-state conditions with little to no fluctuations [2], therefore they can be operated very efficiently. For the design of green processes, the fluctuations need to be taken into account and hence the processes need to be more robust, i.e., the possible window of operation needs to be bigger. Robustness always comes with sub-optimality in a sense that the design needs to be more conservative [18]. This problem can be tackled by means of a multistage reactor design,

as shown by Fischer et al. for methanation processes [19,20]. In the present paper, this concept is explored for methanol production.

This study aims at the robust optimization [18,21] of the operating conditions of a multistage reactor, consisting of three continuously stirred tank reactors, for the production of green methanol, where fluctuations in the hydrogen supply are taken into account. As stated above, a robust design always leads to conservative processes. Furthermore, neglecting the dynamic behavior of the process during robust optimization may lead to infeasible dynamic processes due to transient effects. A feed-forward control scheme consisting of a dynamic optimization in a short time horizon is proposed to overcome this limitation by manipulating the feed distribution and the shell temperatures.

The paper is structured as follows: The required model equations, assumptions, parameters, and the optimization problems are presented in Section 2. The obtained results are shown and discussed in Section 3. Finally, a short summary of the study, the results, and concluding remarks are given in Section 4.

2. Materials and Methods

The process investigated in this work is a heterogeneously catalyzed methanol synthesis using a conventional $Cu/ZnO/Al_2O_3$ catalyst. The process is widely used in industry, with operating conditions between [50, 60] bar and around 250 °C, typically in fixed-bed reactors [2,22,23].

2.1. Kinetic Model

The following three overall reactions take place:

$$CO + 2\,H_2 \rightleftharpoons CH_3OH, \tag{1}$$

$$CO_2 + 3\,H_2 \rightleftharpoons CH_3OH + H_2O, \tag{2}$$

$$CO + H_2O \rightleftharpoons CO_2 + H_2, \tag{3}$$

where Equation (1) is the CO hydrogenation, Equation (2) is the CO_2 hydrogenation, and Equation (3) is the water gas shift reaction.

Established catalysts and kinetics are efficient for feeds consisting mainly of CO, which is also applied in this paper. This implies a two step process, where first CO_2 is converted to CO, which is then converted to methanol [24].

The reaction kinetics is taken from Seidel et al. [25,26], with parameters taken from [27] and given in Table 1. It is modeled as a Langmuir–Hinshelwood kinetics with three types of catalyst centers: heterolytic (het), reduced (red), and oxidized (oxi). The availability of those centers depends on the oxidization state of the catalyst, ϕ. As different centers are necessary for the three reactions, there is a direct influence of the catalyst state on the reaction rates $\boldsymbol{r}$,

$$r_{CO} = (1-\phi)\cdot k_1 \cdot \left(p_{CO} \cdot p_{H_2}^2 - \frac{p_{CH_3OH}}{K_1} \right) \cdot \Theta^{(oxi)} \cdot \Theta^{(het)^4}, \tag{4}$$

$$r_{CO_2} = \phi^2 \cdot k_2 \cdot \left(p_{CO_2} \cdot p_{H_2} - \frac{p_{CH_3OH} \cdot p_{H_2O}}{K_2 \cdot p_{H_2}} \right) \cdot \Theta^{(red)^2} \cdot \Theta^{(het)^4}, \tag{5}$$

$$r_{WGS} = \frac{\phi}{1-\phi} \cdot k_3 \cdot \left(p_{CO_2} - \frac{p_{CO} \cdot p_{H_2O}}{K_3 \cdot p_{H_2}} \right) \cdot \Theta^{(red)} \cdot \Theta^{(oxi)}, \tag{6}$$

where $\boldsymbol{p}$ are the partial pressures of components $i \in [CH_3OH, CO_2, CO, H_2, H_2O]$, $\boldsymbol{K}$ are temperature dependent equilibrium constants,

$$\log(\boldsymbol{K}) = \boldsymbol{\alpha_1} + \boldsymbol{\alpha_2}/T + \boldsymbol{\alpha_3} \cdot \log(T) + \boldsymbol{\alpha_4} \cdot T + \boldsymbol{\alpha_5} \cdot T^2, \tag{7}$$

and k_j are temperature dependent reaction rate constants for reactions $j \in [\mathrm{CO}, \mathrm{CO_2}, \mathrm{WGS}]$,

$$k_j = \exp\left(\mathrm{A}_j - \mathrm{B}_j \cdot \left(\frac{\mathrm{T_{ref}}}{T} - 1\right)\right), \tag{8}$$

with $\mathrm{T_{ref}} = 523.15\,\mathrm{K}$. The relative number of available catalyst centers can be calculated with

$$\Theta^{(\mathrm{oxi})} = \left(1 + \beta_{\mathrm{CO}}^{(\mathrm{oxi})} \cdot p_{\mathrm{CO}}\right)^{-1}, \tag{9}$$

$$\Theta^{(\mathrm{red})} = \left(1 + \beta_{\mathrm{H_2}}^{(\mathrm{red})} \cdot p_{\mathrm{H_2}}^{0.5}\right)^{-1}, \tag{10}$$

$$\Theta^{(\mathrm{het})} = \left(1 + \beta_{\mathrm{CO_2}}^{(\mathrm{het})} \cdot p_{\mathrm{CO_2}}\right)^{-1}. \tag{11}$$

The parameters $\boldsymbol{\beta}$ were fit to experimental data by Seidel et al. [27]. Note that terms with parameters equal to 0 in [27] are neglected here. For a refit of the kinetics, the full version would be required.

Table 1. Parameter values for reaction kinetics model [27].

Parameter	Value	Parameter	Value	Parameter	Value	Unit
$\alpha_{1,1}$	13.814	$\alpha_{1,2}$	15.0921	$\alpha_{1,3}$	1.2777	-
$\alpha_{2,1}$	3784.4	$\alpha_{2,2}$	1581.7	$\alpha_{2,3}$	-2.167	-
$\alpha_{3,1}$	-9.2833	$\alpha_{3,2}$	-8.7639	$\alpha_{3,3}$	0.5194	-
$\alpha_{4,1}$	$3.1475 \cdot 10^{-3}$	$\alpha_{4,2}$	$2.1105 \cdot 10^{-3}$	$\alpha_{4,3}$	$-1.037 \cdot 10^{-3}$	-
$\alpha_{5,1}$	$-4.2613 \cdot 10^{-7}$	$\alpha_{5,2}$	$-1.9303 \cdot 10^{-7}$	$\alpha_{5,3}$	$2.331 \cdot 10^{-7}$	-
$\mathrm{A_{CO}}$	-5.001	$\mathrm{A_{CO_2}}$	-3.145	$\mathrm{A_{WGS}}$	-4.4526	$\mathrm{mol\,bar^{-3}\,kg_{cat}^{-1}\,s^{-1}}$
$\mathrm{B_{CO}}$	26.455	$\mathrm{B_{CO_2}}$	1.5308	$\mathrm{B_{WGS}}$	15.615	-
$\beta_{\mathrm{H_2}}^{(\mathrm{red})}$	1.1064	-	-	-	-	$\mathrm{bar^{-0.5}}$
$\beta_{\mathrm{CO}}^{(\mathrm{oxi})}$	0.14969	$\beta_{\mathrm{CO_2}}^{(\mathrm{het})}$	0.062881	-	-	$\mathrm{bar^{-1}}$
ΔG_1	335.7	ΔG_2	21841.5	-	-	$\mathrm{J\,mol^{-1}}$
k_1^+	$79.174 \cdot 10^{-4}$	k_2^+	$0.188 \cdot 10^{-4}$	-	-	$\mathrm{s^{-1}}$
$\phi_{\max}$	0.9	-	-	-	-	-

Finally, the differential equation to describe the oxidization state of the catalyst reads

$$\frac{\mathrm{d}\phi}{\mathrm{d}t} = k_1^+ \cdot \left(y_{\mathrm{CO}} \cdot \Delta\phi - \gamma_1^{-1} \cdot y_{\mathrm{CO_2}} \cdot \phi\right) + k_2^+ \cdot \left(y_{\mathrm{H_2}} \cdot \Delta\phi - \gamma_2^{-1} \cdot y_{\mathrm{H_2O}} \cdot \phi\right), \tag{12}$$

where y_i are the mole fractions of component i, $\Delta\phi = \phi_{\max} - \phi$, and

$$\gamma = \exp\left(\frac{-\boldsymbol{\Delta G}}{\mathrm{R} \cdot T}\right). \tag{13}$$

The kinetics were fitted to steady-state and dynamical experiments conducted in a micro-Berty reactor. This reactor type resembles a good approximation of an ideally mixed continuous stirred tank reactor (CSTR).

In contrast to traditional kinetic models for methanol synthesis [28–30], dynamic changes of the catalyst are taken into account (Equation (12)), therefore the model is also able to reproduce the transient behavior [25].

2.2. Reactor Model

We consider a non-isothermal CSTR under constant pressure. In the following description of the reactor model, the species are denoted by subscripts i and k, the reactions are denoted by subscript j. The gas and solid phases are denoted by superscript G and S, respectively. The derivation of the material balances follows that of Seidel et al. [27] closely.

However, note that in the present work the temperature also changes with time, hence the equations have to be adopted accordingly.

We start with the component material balance,

$$\frac{\mathrm{d}}{\mathrm{d}t}\left(n_i^{\mathrm{G}} + n_i^{\mathrm{S}}\right) = \dot{n}_{\mathrm{in}} \cdot y_{i,\mathrm{in}} - \dot{n}_{\mathrm{out}} \cdot y_i + m_{\mathrm{cat}} \cdot \sum_j \nu_{i,j} \cdot r_j, \tag{14}$$

with,

$$n_i^{\mathrm{G}} = n^{\mathrm{G}} \cdot y_i, \tag{15}$$

$$n^{\mathrm{G}} = \frac{\mathrm{p} \cdot \mathrm{V}}{\mathrm{R} \cdot T}, \quad \dot{n}_{\mathrm{out}} = \frac{\mathrm{p} \cdot \dot{V}_{\mathrm{out}}}{\mathrm{R} \cdot T}, \quad \dot{n}_{\mathrm{in}} = \frac{\mathrm{p} \cdot \dot{V}_{\mathrm{in}}}{\mathrm{R} \cdot T_{\mathrm{in}}}, \tag{16}$$

$$n_i^{\mathrm{S}} = \mathrm{m}_{\mathrm{cat}} \cdot \mathrm{q}_{\mathrm{sat}} \cdot \Theta_i, \tag{17}$$

$$\Theta_i = p_i \cdot \sum_l \beta_i^l \cdot \Theta^l, \quad l \in [(\mathrm{oxi}), (\mathrm{red}), (\mathrm{het})], \tag{18}$$

where $\boldsymbol{y}$ are the molar fractions, $\boldsymbol{\nu}$ are the stoichiometric coefficients, the reactor's pressure, volume, and temperature are given by p, V , and T, respectively, $\dot{V}_{\mathrm{out}}$ is the volumetric outlet flow-rate, $\dot{V}_{\mathrm{in}}$ is the feed flow rate, T_{in} is the feed temperature, $\mathrm{m}_{\mathrm{cat}}$ is the catalyst mass, $\mathrm{q}_{\mathrm{sat}}$ is the adsorption capacity of the catalyst, and $\boldsymbol{\Theta}$ are competitive Langmuir adsorption isotherms, which depend on the partial pressures of the species. Details are given in [31]. The reactor temperature T is equal to the outlet temperature, hence the subscript "out" will be neglected for better readability. Note that all $\boldsymbol{\beta_i}$ in Equation (18) not used in Equations (9)–(11) are equal to 0.

The time derivatives for n_i^{G}, and n_i^{S} are given by

$$\frac{\mathrm{d}n_i^{\mathrm{S}}}{\mathrm{d}t} = \mathrm{m}_{\mathrm{cat}} \cdot \mathrm{q}_{\mathrm{sat}} \cdot \sum_k \frac{\partial \Theta_i}{\partial p_k} \cdot \frac{\mathrm{d}p_k}{\mathrm{d}t}, \tag{19}$$

$$\frac{\mathrm{d}n_i^{\mathrm{G}}}{\mathrm{d}t} = \frac{\partial n^{\mathrm{G}}}{\partial T} \cdot \frac{\mathrm{d}T}{\mathrm{d}t} \cdot y_i + n^{\mathrm{G}} \cdot \frac{\mathrm{d}y_i}{\mathrm{d}t}; \tag{20}$$

an explicit calculation of the partial derivatives of the adsorption isotherms, $\frac{\partial \Theta_i}{\partial p_k}$, can be found in the Appendix of Nikolić et al. [31].

Introducing Equations (19) and (20) into Equation (14),

$$\begin{aligned} &\frac{\partial n^{\mathrm{G}}}{\partial T} \cdot \frac{\mathrm{d}T}{\mathrm{d}t} \cdot y_i + n^{\mathrm{G}} \cdot \frac{\mathrm{d}y_i}{\mathrm{d}t} + \mathrm{m}_{\mathrm{cat}} \cdot q_{\mathrm{sat}} \cdot \mathrm{p} \cdot \sum_k \frac{\partial \Theta_i}{\partial p_k} \cdot \frac{\mathrm{d}y_k}{\mathrm{d}t} = \\ &\dot{n}_{\mathrm{in}} \cdot y_{i,\mathrm{in}} - \dot{n}_{\mathrm{out}} \cdot y_i + \mathrm{m}_{\mathrm{cat}} \cdot \sum_j \nu_{i,j} \cdot r_j, \end{aligned} \tag{21}$$

and summation over the single species yields the total material balance,

$$\frac{\partial n^{\mathrm{G}}}{\partial T} \cdot \frac{\mathrm{d}T}{\mathrm{d}t} + \mathrm{m}_{\mathrm{cat}} \cdot \mathrm{q}_{\mathrm{sat}} \cdot \mathrm{P} \cdot \sum_i \sum_k \frac{\partial \Theta_i}{\partial p_k} \cdot \frac{\mathrm{d}y_k}{\mathrm{d}t} = \dot{n}_{\mathrm{in}} - \dot{n}_{\mathrm{out}} + \mathrm{m}_{\mathrm{cat}} \cdot \sum_i \sum_j \nu_{i,j} \cdot r_j. \tag{22}$$

Solving Equation (22) for $\dot{n}_{\mathrm{out}}$ to eliminate it in Equation (21) yields the component material balance in its final form,

$$\begin{aligned} &n^{\mathrm{G}} \cdot \frac{\mathrm{d}y_i}{\mathrm{d}t} + \mathrm{m}_{\mathrm{cat}} \cdot \mathrm{q}_{\mathrm{sat}} \cdot \mathrm{p} \cdot \left(\sum_k \frac{\partial \Theta_i}{\partial p_k} \cdot \frac{\mathrm{d}y_k}{\mathrm{d}t} - \sum_i \sum_k \left(\frac{\partial \Theta_i}{\partial p_k} \cdot \frac{\mathrm{d}y_k}{\mathrm{d}t} \right) \cdot y_i \right) = \\ &\dot{n}_{\mathrm{in}} \cdot (y_{i,\mathrm{in}} - y_i) + \mathrm{m}_{\mathrm{cat}} \cdot \left(\sum_j \nu_{i,j} \cdot r_j - \sum_i \sum_j (\nu_{i,j} \cdot r_j) \cdot y_i \right). \end{aligned} \tag{23}$$

Note that Equation (23), in contrast to Equations (21) and (22), is identical to that obtained assuming a constant reactor temperature [27], i.e., the component material balance is not temperature-dependent. However, the volumetric outlet flow rate (which can be derived from Equation (22)) differs, as it is temperature dependent,

$$\dot{V}_{\mathrm{out}} = \frac{\mathrm{V}}{T} \cdot \frac{\mathrm{d}T}{\mathrm{d}t} + \frac{T}{T_{\mathrm{in}}} \dot{V}_{\mathrm{in}} + \frac{\mathrm{m_{cat}} \cdot \mathrm{R} \cdot T}{\mathrm{p}} \cdot \left(\sum_i \sum_j \nu_{i,j} \cdot r_j - \mathrm{q_{sat}} \cdot \mathrm{p} \cdot \sum_i \sum_k \frac{\partial \Theta_i}{\partial p_k} \cdot \frac{\mathrm{d}y_k}{\mathrm{d}t} \right). \quad (24)$$

2.3. Energy Balance

To describe the change in temperature, an energy balance is required. We start with the total energy balance,

$$\frac{\mathrm{d}}{\mathrm{d}t} \left(\sum_i n_i^{\mathrm{G}} \cdot h_i^{\mathrm{G}} + \sum_i n_i^{\mathrm{S}} \cdot h_i^{\mathrm{S}} + \mathrm{m_{cat}} \cdot h_{\mathrm{cat}}^{*} \right) = \dot{n}_{\mathrm{in}} \cdot \sum_i h_{i,\mathrm{in}}^{\mathrm{G}} \cdot y_{i,\mathrm{in}} - \dot{n}_{\mathrm{out}} \cdot \sum_i h_i^{\mathrm{G}} \cdot y_i - \dot{Q}_{\mathrm{c}}, \quad (25)$$

where $\boldsymbol{h}$ are enthalpies, and $\dot{Q}_{\mathrm{c}}$ is the cooling. Applying the product rule, introducing $\mathrm{d}h_{\mathrm{cat}}^{*} = \mathrm{c_p^{cat}} \mathrm{d}T$, and assuming constant $\mathrm{m_{cat}}$, and $\mathrm{c_p^{cat}}$ yields

$$\begin{aligned} \sum_i \frac{\mathrm{d}n_i^{\mathrm{G}}}{\mathrm{d}t} \cdot h_i^{\mathrm{G}} + \sum_i n_i^{\mathrm{G}} \cdot \frac{\mathrm{d}h_i^{\mathrm{G}}}{\mathrm{d}t} + \sum_i \frac{\mathrm{d}n_i^{\mathrm{S}}}{\mathrm{d}t} \cdot h_i^{\mathrm{S}} + \sum_i n_i^{\mathrm{S}} \cdot \frac{\mathrm{d}h_i^{\mathrm{S}}}{\mathrm{d}t} + \mathrm{m_{cat}} \cdot \mathrm{c_p^{cat}} \frac{\mathrm{d}T}{\mathrm{d}t} = \\ \dot{n}_{\mathrm{in}} \cdot \sum_i h_{i,\mathrm{in}} \cdot y_{i,\mathrm{in}} - \dot{n}_{\mathrm{out}} \cdot \sum_i h_i^{\mathrm{G}} \cdot y_i - \dot{Q}_{\mathrm{c}}. \end{aligned} \quad (26)$$

To simplify the equation, the component material balance, Equation (14), is multiplied with the component gas enthalpies, h_i^{G}, summed over i, and solved for

$$\begin{aligned} \sum_i \frac{\mathrm{d}n_i^{\mathrm{G}}}{\mathrm{d}t} \cdot h_i^{\mathrm{G}} = &- \sum_i \frac{\mathrm{d}n_i^{\mathrm{S}}}{\mathrm{d}t} \cdot h_i^{\mathrm{G}} + \dot{n}_{\mathrm{in}} \cdot \sum_i h_i^{\mathrm{G}} \cdot y_{i,\mathrm{in}} \\ &- \dot{n}_{\mathrm{out}} \cdot \sum_i h_i^{\mathrm{G}} \cdot y_i + \mathrm{m_{cat}} \sum_j \Delta h_{\mathrm{R},j} \cdot r_j, \end{aligned} \quad (27)$$

where $\Delta h_{\mathrm{R},j}$ is the heat of reaction j. Putting this into Equation (26) yields

$$\begin{aligned} \sum_i n_i^{\mathrm{G}} \cdot \frac{\mathrm{d}h_i^{\mathrm{G}}}{\mathrm{d}t} + \sum_i \frac{\mathrm{d}n_i^{\mathrm{S}}}{\mathrm{d}t} \cdot \left(h_i^{\mathrm{S}} - h_i^{\mathrm{G}} \right) + \sum_i n_i^{\mathrm{S}} \cdot \frac{\mathrm{d}h_i^{\mathrm{S}}}{\mathrm{d}t} + \mathrm{m_{cat}} \cdot c_{\mathrm{p}}^{\mathrm{cat}} \frac{\mathrm{d}T}{\mathrm{d}t} = \\ \dot{n}_{\mathrm{in}} \cdot \sum_i \left(h_{i,\mathrm{in}}^{\mathrm{G}} - h_i^{\mathrm{G}} \right) \cdot y_{i,\mathrm{in}} - \mathrm{m_{cat}} \sum_j \Delta h_{\mathrm{R},j} \cdot r_j - \dot{Q}_{\mathrm{c}}. \end{aligned} \quad (28)$$

The enthalpies can be described by

$$h_i = \int_{\mathrm{T_{ref}}}^{T} c_{\mathrm{p},i}(T) \mathrm{d}T + \Delta \mathrm{h_{f,ref,}}_i, \quad (29)$$

where $\Delta \mathrm{h_{f,ref,}}_i$ is the heat of formation and $\boldsymbol{c}_{\mathrm{p}}$ is the isobaric heat capacity. We assume that $\boldsymbol{c}_{\mathrm{p}}^{\mathrm{S}}$ does not depend on the temperature, a correlation for $\boldsymbol{c}_{\mathrm{p}}^{\mathrm{G}}$ in $\mathrm{J\,mol^{-1}\,K^{-1}}$,

$$c_{\mathrm{p,i}}^{\mathrm{G}} = \Gamma_{1,i} + \Gamma_{2,i} \cdot T + \Gamma_{3,i} \cdot T^2 + \Gamma_{4,i} \cdot T^3, \quad (30)$$

as well as values for $\Delta \mathbf{h}_{\mathrm{f,ref}}$ and $\boldsymbol{\Gamma}$, given in Table 2, can be found in [32].

With that, and by introducing the heat of cooling, the following equation can be obtained for the change in temperature:

$$\left(\underbrace{n^{\mathrm{G}} \cdot \bar{c}_{\mathrm{p}}^{\mathrm{G}}}_{\text{gaseous species}} + \underbrace{\cancelto{0}{\mathrm{m}_{\mathrm{cat}} \cdot \eta_{\mathrm{sat}} \cdot \bar{c}_{\mathrm{p}}^{\mathrm{S}}}}_{\text{adsorbed species}} + \underbrace{\mathrm{m}_{\mathrm{cat}} \cdot c_{\mathrm{p}}^{\mathrm{cat}}}_{\text{"dead" catalyst}} \right) \cdot \frac{\mathrm{d}T}{\mathrm{d}t} = \\ \underbrace{- \dot{n}_{\mathrm{in}} \cdot \sum_i \int_{T_{\mathrm{in}}}^{T} c_{\mathrm{p},i}^{\mathrm{G}} \, \mathrm{d}T \cdot y_{i,\mathrm{in}}}_{\text{heat of transport}} \underbrace{- \mathrm{m}_{\mathrm{cat}} \sum_j \Delta h_{\mathrm{R},j} \cdot r_j}_{\text{heat of reaction}} \underbrace{- \mathrm{K}_{\mathrm{W}} \cdot \mathrm{A}_{\mathrm{W}} \cdot (T - T_{\mathrm{c}})}_{\text{heat of cooling}} \underbrace{- \sum_i \frac{\mathrm{d}n_i^{\mathrm{S}}}{\mathrm{d}t} \cdot \Delta \mathrm{h}_{\mathrm{ads},i}}_{\text{heat of adsorption}}, \tag{31}$$

with

$$\bar{c}_{\mathrm{p}}^{\mathrm{G}} = \sum_i c_{\mathrm{p},i}^{\mathrm{G}} \cdot y_i, \quad \Delta \mathrm{h}_{\mathrm{ads},i} = h_i^{\mathrm{S}} - h_i^{\mathrm{G}}. \tag{32}$$

The adsorption enthalpy is assumed to be constant and identical for each component, with $\Delta \mathbf{h}_{\mathrm{ads}} = 1 \cdot 10^3 \, \mathrm{J \, mol^{-1}}$. Note that, since the heat of adsorption is relatively small compared to the heat of reaction, only a rough estimate is used.

Table 2. Thermodynamic data, taken from Appendix A of Reid et al. [32]; $\Delta \mathrm{h}_{\mathrm{f,ref},i}$ in $\mathrm{J \, mol^{-1}}$; reference temperature for $\Delta \mathrm{h}_{\mathrm{f,ref},i}$: $\mathrm{T_{ref}} = 298.2 \, \mathrm{K}$.

Species	$\boldsymbol{\Gamma_{1,i}}$	$\boldsymbol{\Gamma_{2,i}}$	$\boldsymbol{\Gamma_{3,i}}$	$\boldsymbol{\Gamma_{4,i}}$	$\boldsymbol{\Delta h_{\mathrm{f,ref},i}}$
CH_3OH	$2.115 \cdot 10^1$	$7.092 \cdot 10^{-2}$	$2.587 \cdot 10^{-5}$	$-2.852 \cdot 10^{-8}$	$-2.013 \cdot 10^5$
CO_2	$1.980 \cdot 10^1$	$7.344 \cdot 10^{-2}$	$-5.602 \cdot 10^{-5}$	$1.715 \cdot 10^{-8}$	$-3.938 \cdot 10^5$
CO	$3.087 \cdot 10^1$	$-1.285 \cdot 10^{-2}$	$2.789 \cdot 10^{-5}$	$-1.272 \cdot 10^{-8}$	$-1.106 \cdot 10^5$
H_2	$2.714 \cdot 10^1$	$9.274 \cdot 10^{-3}$	$-1.381 \cdot 10^{-5}$	$7.645 \cdot 10^{-9}$	0
H_2O	$3.224 \cdot 10^1$	$1.924 \cdot 10^{-3}$	$1.055 \cdot 10^{-5}$	$-3.596 \cdot 10^{-9}$	$-2.420 \cdot 10^5$

2.4. Multistage Reactor

The considered process is depicted in Figure 1. The multistage reactor consists of three CSTR with side-feeds for each reactor, which can be seen as an approximation of a staged multibed reactor. For CO_2 methanation, it is demonstrated in [19,20] that such a feed split increases robustness against fluctuations. The idea is transferred here to methanol production from CO. A different concept of a staged fixed bed reactor for methanol production from CO_2 was studied by Torcida et al. [33]. There, intermediate cooling without feed split between the different stages is used to increase reactor efficiency.

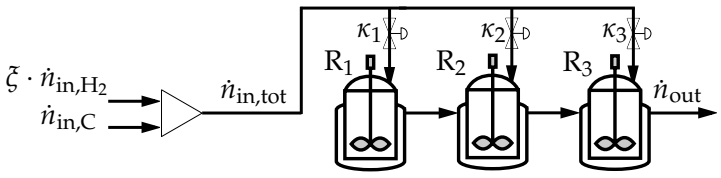

Figure 1. Process flowsheet.

We consider 3 reactors within the setup; they will be denoted by the subscript $r \in [1, 2, 3]$ in the following.

The feed is split by a split-ratio, $\boldsymbol{\kappa}$, with

$$\dot{n}_{\mathrm{in},1} = \kappa_1 \cdot \dot{n}_{\mathrm{in,tot}}, \tag{33}$$

$$\dot{n}_{\mathrm{in},\bar{r}} = \kappa_{\bar{r}} \cdot \dot{n}_{\mathrm{in,tot}} + \dot{n}_{\mathrm{out},\bar{r}-1}, \quad \bar{r} \in [2, 3], \tag{34}$$

$$\sum_r \kappa_r = 1, \tag{35}$$

where $\dot{n}_{\text{in,tot}}$ is the total volumetric inlet flow into the system. It consists of the fluctuating hydrogen stream, $\xi \cdot \dot{n}_{H_2,in,tot}$, and a carbon stream, $\dot{n}_{C,in,tot}$, its composition and amount is calculated with

$$\dot{n}_{\text{in,tot}} = \xi \cdot \dot{n}_{\text{H}_2,\text{in,tot}} + \dot{n}_{\text{C,in,tot}}, \tag{36}$$

$$y_{\text{H}_2,\text{in,tot}} = \frac{\xi \cdot \dot{n}_{\text{H}_2,\text{in,tot}}}{\dot{n}_{\text{in,tot}}}, \tag{37}$$

$$y_{\text{CO}_2,\text{in,tot}} = \frac{\dot{n}_{\text{C,in,tot}} \cdot \psi_{\text{C}}}{\dot{n}_{\text{in,tot}}}, \tag{38}$$

$$y_{\text{CO,in,tot}} = \frac{\dot{n}_{\text{C,in,tot}} \cdot (1 - \psi_{\text{C}})}{\dot{n}_{\text{in,tot}}}, \tag{39}$$

The inlet compositions and temperatures for reactors 2 and 3 are calculated accordingly with

$$\boldsymbol{y}_{\text{in},\bar{r}} = \frac{\boldsymbol{y}_{\bar{r}-1} \cdot \dot{n}_{\text{out},\bar{r}-1} + \kappa_{\bar{r}} \cdot \dot{n}_{\text{in,tot}} \cdot \boldsymbol{y}_{\text{in,tot}}}{\dot{n}_{\text{out},\bar{r}-1} + \kappa_{\bar{r}} \cdot \dot{n}_{\text{in,tot}}}, \tag{40}$$

$$T_{\text{in},\bar{r}} = \frac{T_{\bar{r}-1} \cdot \dot{n}_{\text{out},\bar{r}-1} + \kappa_{\bar{r}} \cdot \dot{n}_{\text{in,tot}} \cdot T_{\text{in,tot}}}{\dot{n}_{\text{out},\bar{r}-1} + \kappa_{\bar{r}} \cdot \dot{n}_{\text{in,tot}}}, \tag{41}$$

where $T_{\text{in,tot}}$ is the temperature of the inlet into the system. Note that the inlet temperature and inlet composition for stage $\bar{r}$ are mean values based on the mole amounts of the entering streams, hence those values are estimates.

The reactors are parameterized such that the overall system resembles an industrial scale reactor. The heat transfer coefficient, K_W, was approximated according to [34,35]. The parameters are given in Table 3. The overall reactor volume and catalyst mass are split equally,

$$\text{V}_r = \frac{\text{V}_\text{tot}}{3}, \tag{42}$$

$$m_{\text{cat},r} = \frac{\text{m}_\text{cat,tot}}{3}. \tag{43}$$

Table 3. Reactor parameters.

Parameter	Value	Unit
V_tot	2.83	m^3
P	70	bar
K_W	250	$\text{W m}^{-2}\,\text{K}^{-1}$
A_W	18.85	m^2
q_sat	0.98	mol kg^{-1}
$\text{c}_\text{p}^\text{cat}$	1063	$\text{J kg}^{-1}\,\text{K}^{-1}$
$\text{m}_\text{cat,tot}$	2002	kg
ρ_cat	1770	kg m^{-3}

2.5. Optimization Approach

We consider three optimization problems. The first one is the nominal steady-state optimization problem,

$$\begin{aligned} \max_{\boldsymbol{x}} \quad & J = STY(\boldsymbol{x})^2, \\ \text{s. t.} \quad & \text{Equations (4)–(43) in steady-state,} \\ & \boldsymbol{x}^{\text{lo}} \leq \boldsymbol{x} \leq \boldsymbol{x}^{\text{up}}, \\ & X_{\text{C}}(\boldsymbol{x}) \geq 0.6, \\ & (\boldsymbol{T}(\boldsymbol{x}) - \boldsymbol{T}_c)^2 \leq 30^2, \\ & \sum_i y_i(\boldsymbol{x}) = 1, \\ & \sum_i y_{i,\text{in,tot}} = 1, \\ & y_{\text{CO,in,tot}} + y_{\text{CO}_2\text{,in,tot}} \geq 0.01, \end{aligned} \tag{44}$$

where $\boldsymbol{x} \in G \subseteq \mathbb{R}^d$ are variables with upper ($\boldsymbol{x}^{\text{up}}$) and lower bounds ($\boldsymbol{x}^{\text{lo}}$). The space–time yield is defined as

$$STY = \left(\frac{\dot{n}_{\text{out,4}} \cdot y_{\text{CH}_3\text{OH,4}}}{\text{V}_{\text{tot}}} \right), \tag{45}$$

and the carbon conversion is defined as

$$X_{\text{C}} = \frac{y_{\text{CH}_3\text{OH,4}} \cdot \dot{n}_{\text{out,4}}}{\dot{n}_{\text{C,in,tot}}}, \tag{46}$$

upper and lower bounds for the variables are given in Table 4. We enforce a specific carbon conversion rate, while carbon conversion and the objective of a maximized space–time yield are concurrent. This also leads to higher reactor temperatures, as the reaction is exothermic. To prevent hotspot formation, there is a restriction on the differences between the reactor temperatures and the shell temperatures in Problem 1 (44) [36].

The second problem is the robust steady-state optimization,

$$\begin{aligned} \max_{\boldsymbol{x}} \quad & J = \mathbb{E}_{\xi}\left(STY(\boldsymbol{x}, \xi)^2\right), \\ \text{s. t.} \quad & \text{Equations (4)–(43) in steady-state,} \\ & \boldsymbol{x}^{\text{lo}} \leq \boldsymbol{x} \leq \boldsymbol{x}^{\text{up}}, \\ & X_{\text{C}}(\boldsymbol{x}, \xi) \geq 0.6, \\ & (\boldsymbol{T}(\boldsymbol{x}, \xi) - \boldsymbol{T}_c)^2 \leq 30^2, \\ & \sum_i y_i(\boldsymbol{x}, \xi) = 1, \\ & \sum_i y_{i,\text{in,tot}} = 1, \\ & y_{\text{CO,in,tot}} + y_{\text{CO}_2\text{,in,tot}} \geq 0.01, \end{aligned} \tag{47}$$

where the space–time yield is maximized with the same constraints as in Problem 1 (44), but with taking fluctuations into account (see the left plot of Figure 2): $\xi \in [0.75, 1.25]$ is the disturbance of H_2 at the inlet, the problem is discretized along ξ using 50 equally distant distributed support points. It is assumed that the carbon source is able to deliver CO and CO_2 as needed, but the hydrogen source is prone to fluctuations due to its renewable character, i.e., hydrogen is produced via electrolysis using wind energy. Each support point of ξ refers to a different scenario with a given disturbance rate. The problem is solved simultaneously, i.e., the optimizer identifies an optimal solution that holds the constraints for each support point of ξ.

Note that we only consider steady-state scenarios of the process here. Transient behavior that may occur when changing from one disturbance to another is neglected in this step.

The third optimization problem is a dynamic optimization, where the design parameters of the reactor setup are fixed. Only operating conditions, i.e., the feed split and the shell temperatures, may be changed dynamically. The problem is defined as:

$$\begin{aligned}
\max_{\boldsymbol{x}} \quad & J = \int STY(\boldsymbol{x},\xi)^2 / t_{\text{end}}^2 - \mathrm{U}\cdot(s_1+s_2)\,\mathrm{d}t \\
\text{s.t.} \quad & \text{Equations (4)–(43)}, \\
& \boldsymbol{x}^{\text{lo}} \le \boldsymbol{x} \le \boldsymbol{x}^{\text{up}}, \\
& X_{\mathrm{C}}(\boldsymbol{x},\xi) + s_1 \ge 0.6, \\
& (\boldsymbol{T}(\boldsymbol{x},\xi) - \boldsymbol{T}_c)^2 \le (30+s_2)^2, \\
& \sum_i y_i(\boldsymbol{x},\xi) = 1, \\
& \sum_i y_{i,\text{in}} = 1, \\
& \dot{\boldsymbol{T}}_c = \frac{-\boldsymbol{T}_c + \boldsymbol{T}_{c,s}}{50}, \\
& \dot{\boldsymbol{\kappa}} = \frac{-\boldsymbol{\kappa} + \boldsymbol{\kappa}_s}{15},
\end{aligned} \tag{48}$$

where $\boldsymbol{s}$ are slack variables, and $\mathrm{U} = 100$ is a heuristically set penalty constant. The slack variables allow for violation of the constraints at the expense of a highly reduced cost function, hence the optimizer tries to avoid this as much as possible.

Table 4. Variables and respective bounds. Variables below the mid rule are degrees of freedom. Degrees of freedom marked with "$*$" may change during the dynamic optimization.

Variable	Domain	Unit	Description
$\boldsymbol{T}$	$[480, 573]$	K	Reactor temperature
$\dot{V}_{\text{out}}$	$[1{\cdot}10^{-4}, 5{\cdot}10^{-1}]$	$\mathrm{m^3\,s^{-1}}$	Volumetric outlet flowrate
$y_{\mathrm{CO,in}}$	$[0, 0.5]$	-	CO inlet mole fraction
$y_{\mathrm{CO_2,in}}$	$[0, 0.5]$	-	CO_2 inlet mole fraction
$y_{\mathrm{H_2,in}}$	$[0.5, 0.85]$	-	H_2 inlet mole fraction
$\boldsymbol{T}_{\mathrm{c}}^*$	$[490, 550]$	K	Cooling temperature
$\boldsymbol{T}_{\mathrm{c,s}}^*$	$[490, 550]$	K	Cooling temperature setpoint
$T_{\mathrm{in,tot}}$	$[490, 520]$	K	System feed temperature
$\dot{n}_{\mathrm{C,in,tot}}$	$[1, 300]$	$\mathrm{mol\,s^{-1}}$	System inlet carbon molar flow
$\dot{n}_{\mathrm{H_2,in,tot}}$	$[1, 300]$	$\mathrm{mol\,s^{-1}}$	System inlet hydrogen molar flow
ψ_{C}	$[0, 1]$	-	CO, CO_2 split ratio
$\boldsymbol{\kappa}^*$	$[0, 1]$	-	Feed split ratio
$\boldsymbol{\kappa}_s^*$	$[0, 1]$	-	Feed split ratio setpoint
s_1^*	$[0, 0.3]$	-	Carbon conversion slack variable
s_2^*	$[0, 10]$	-	Cooling temperature slack variable

Note that additional constraints are present in Problem 3 (48) to determine the dynamic behavior of the feed split and shell temperature. First order lag equations are used to obtain a more realistic result, with time constants of 15 and 50, respectively. Without those lags, the optimizer would be able to change the operating conditions instantly from one extreme to another in the feasible range, giving rise to so-called bang-bang solutions. Although bang-bang solutions may be optimal, they are not achievable in a real application. Variables $\boldsymbol{T}_{\mathrm{c,s}}$, and $\boldsymbol{\kappa}_{\mathrm{c,s}}$ are the setpoints of the lag elements, which are degrees of freedom for the optimizer.

All optimization problems are implemented in Julia [37], using the JuMP [38] based package InfiniteOpt [39]. For Problem 3 (48) an orthogonal collocation of third order [40] with 200 equally distant support points is used for the discretization of the infinite dimensional problem. All three problems are solved using the NLP solver KNITRO [41]; for Problems 1 (44) and 2 (47), the multi-start option is set to 50.

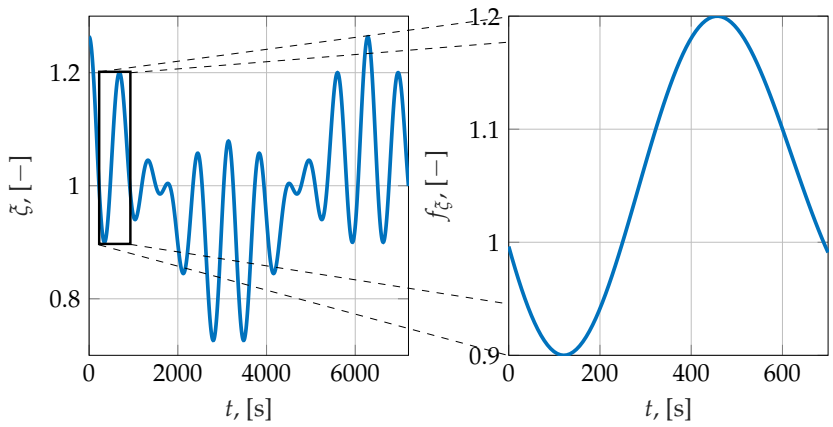

Figure 2. Disturbance test function. (**Left**): whole domain relevant for steady-state optimizations; (**right**): test function for dynamic transient behavior.

2.6. Test Function

A drawback of Problem 2 (47) is that only steady-state realizations are investigated, neglecting the transient behavior when fluctuations occur. The design obtained from Problem 1 (44) does not take fluctuations into account. Therefore, an additional test is required to check whether the imposed constraints are met under dynamically changing disturbances. The employed test function is depicted in the right subplot of Figure 2. It can be described by the following set of equations,

$$\Delta t = t + 226, \quad t \in [0, 700], \tag{49}$$

$$f = \Re(\exp(0.01\mathrm{i} \cdot \Delta t) + \exp(0.001\mathrm{i} \cdot \Delta t) + \exp(0.008\mathrm{i} \cdot \Delta t)), \tag{50}$$

$$f_{\text{norm}} = \frac{f + |\min(f)|}{\max(f + |\min(f))|}, \tag{51}$$

$$f_\xi = |0.9 + f_{\text{norm}} \cdot (0.3)|, \tag{52}$$

where i is the imaginary number, and $\Re(f)$ is the real part of f. The time is shifted such that $f_\xi(t = 0) = 1$. The test function can be interpreted as a complex Fourier series, which is truncated after the third entry and normalized such that the resulting function lies within the desired interval.

Note that the employed test function for dynamic transient behavior does not resemble the worst-case scenario, which would be a series of rectangle steps. Instead, it is modeled such that it resembles real wind fluctuations [42,43] better. However, the presented disturbance fluctuates more rapidly than it would be observed in the real world. Hence, it is a model profile not related to an existing green electricity profile. A short time horizon of this modeled disturbance was arbitrarily chosen as the test function, marked with a black rectangle in the left plot of Figure 2.

The test function is used in a dynamic forward simulation of the obtained reactor setups from Problems 1 (44) and 2 (47), starting at the steady-state of the system.

A linear interpolation is used for the simulation of the design obtained from Problem 2 (47). The feed split ratios in between the support points are interpolated.

The simulation is implemented in Julia using the DifferentialEquations [44] package.

3. Results and Discussion

Two case studies are discussed in this section, one with the nominal reactor obtained from Problem 1 (44) and one with the robust reactor obtained from Problem 2 (47). Both reactor realizations are tested in a simulation framework and are compared to each other. In a last step, the dynamic optimization in Problem 3 (48) is solved for both designs.

3.1. Nominal Steady-State Design

The nominal design is the solution of Problem 1 (44). The obtained optimal values of the degrees of freedom are given in Table 5.

Table 5. Obtained values for degrees of freedom for nominal design, solution of Problem 1 (44).

$\dot{n}_{C,in,tot}$	$\dot{n}_{H_2,in,tot}$	ψ_C	$T_{in,tot}$	T_c	κ	STY
3.67	20.81	0.0125	490	[496, 537, 528]	[0.195, 0.805, 0]	0.78

The lowest possible inlet temperature is chosen. As the reaction is exothermic, the inlet stream acts as a sort of cooling mechanism.

The inlet stream consists mostly of hydrogen, with $y_{H_2,in,tot} = 0.85$. Note that this value lies on the boundary. If no restriction on $y_{H_2,in,tot}$ is present, the value is chosen to be higher, which would be favorable for the temperature management of the reactor setup. However, most of the increased hydrogen stream would leave the reactor unreacted, increasing the overall process cost.

Regarding the feed split, approximately one fifth of the feed is fed into the first reactor and four fifths are fed into the second. The first reactor is relatively cold, which leads to a fast conversion and a high temperature increase; therefore, only a small fraction of the reactants can enter. With increasing temperature, the reaction and heat production slow down. Therefore, most of the feed is fed into the much hotter second reactor, which is not only cooled by the shell, but also by the entering streams. The feed to the third reactor is not used. Feeding the third reactor would reduce the residence time, as the first two reactors are bypassed. This would lead to the production of less methanol, which is unfavorable for the used objective function.

The dynamic simulation results for the nominal reactor design are shown in Figure 3. The figure consists of four subplots: the upper left corner shows the mole fraction of methanol over time, the upper right corner the reactor temperature over time, the lower left corner the molar outlet streams over time, and the lower right corner the carbon conversion rate over time. The fluctuations can be well observed in all of those subplots. It is clear from the lower right subplot that the nominal reactor is not feasible for the present disturbance, as it lies well below the desired carbon conversion of 60%. The obtained space–time yield is $STY = 0.8047$.

3.2. Robust Design

The robust design is the solution of Problem 2 (47). The obtained values of the constant degrees of freedom are given in Table 6, Figure 4 shows the feed split and the resulting carbon conversion rates. Note that the x-axis of Figure 4 is the disturbance.

Table 6. Obtained values for degrees of freedom for robust design, solution of Problem 2 (47).

$\dot{n}_{C,in,tot}$	$\dot{n}_{H_2,in,tot}$	ψ_C	$T_{in,tot}$	T_c	$\mathbb{E}_\xi(STY)$
3.01	13.66	0.014	490	[543, 526, 519]	0.67

The inlet composition is slightly different than for the nominal case. There is proportionally less H_2 fed into the reactor. However, the obtained value for $\dot{n}_{H_2,in,tot}$ leads to a mole fraction of 0.85 for the highest hydrogen inlet increase. There is also slightly more CO_2 present in the inlet stream.

The inlet temperature is, again, chosen to be as small as possible. There is a notable difference between the shell temperatures chosen for the nominal and robust designs. While the shell temperature of the first reactor in the nominal design is very low, it is the highest in the robust design. This can be explained by the feed split. In contrast to the nominal design, most of the feed is fed into the first reactor now.

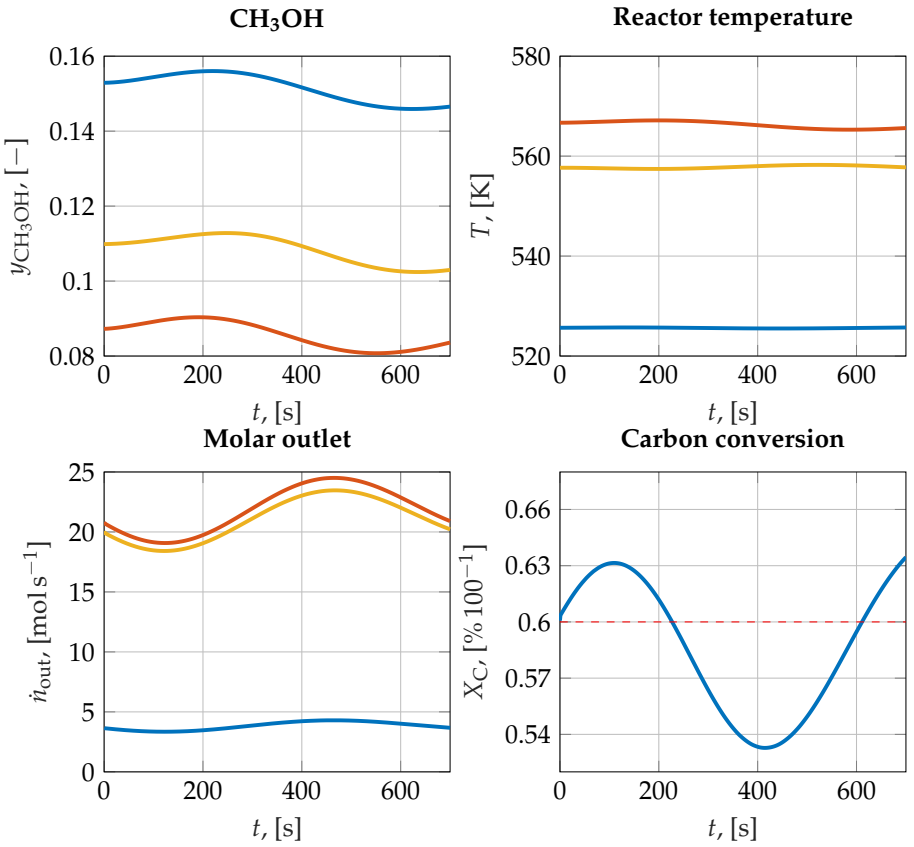

Figure 3. Simulation results for nominal reactor design using f_{ξ} as disturbance. Blue: first reactor, orange: second reactor, yellow: third reactor. The red dashed line in the lower right subplot indicates the required carbon conversion of 60%.

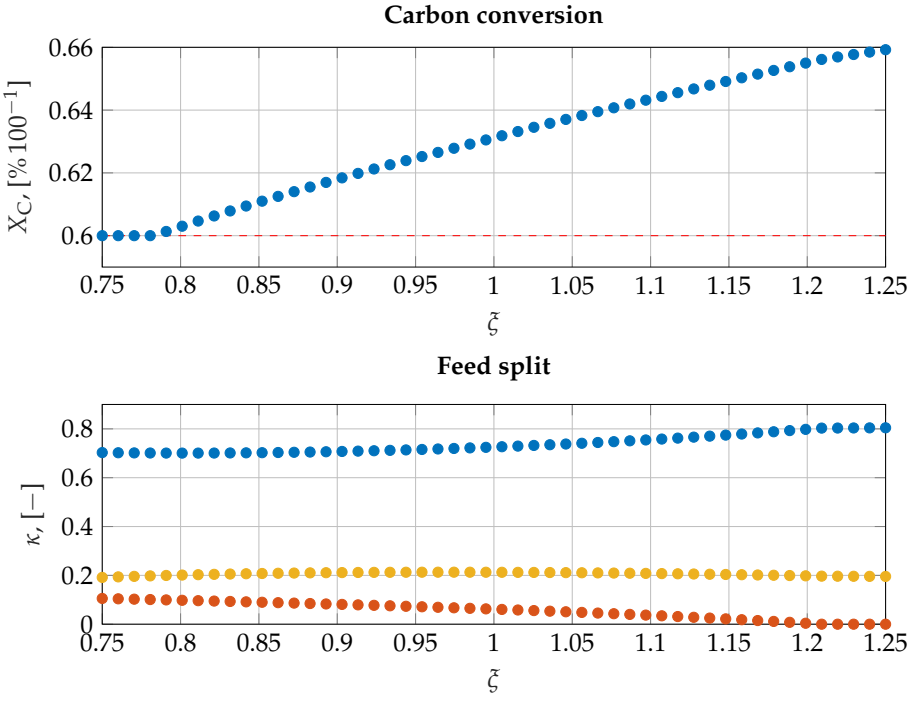

Figure 4. Feed split and steady-state carbon conversion for robust design, solution of Problem 2 (47). Blue: first reactor, orange: second reactor, yellow: third reactor. The red dashed line in the upper subplot indicates the required carbon conversion of 60%.

The feed split changes for different disturbance values, although its main split remains constant: most of the feed goes into reactor 1. Interestingly, some of the feed is fed directly into reactor 3. Note that reactor 3 is the coldest and hence has the fastest reaction rate.

Generally, with increasing hydrogen flows, the steady-state carbon conversion increases and vice versa, as the temperature is reduced by a higher inlet flow, which increases the reaction rate due to the temperature dependence of the equilibrium of the water-gas-shift reaction.

Compared to the nominal design, the mean space–time yield of the robust design is reduced by 14 %. This is to be expected, as the robust design has to be more conservative and hence inefficient.

The dynamic simulation results for the robust reactor design are shown in Figure 5 (the figure has the same layout as Figure 3, described above). Although much better than in the nominal case, the robust design is still infeasible with regard to the carbon conversion, as it lies below the desired 60%. This can be explained by the neglected transient behavior and non-linear dynamics of the model, as Problem 2 (47) only considers a steady-state optimization. The obtained space–time yield is $STY = 0.7037$, which is 12.6% less than in the nominal case and the price we have to pay for the increased robustness.

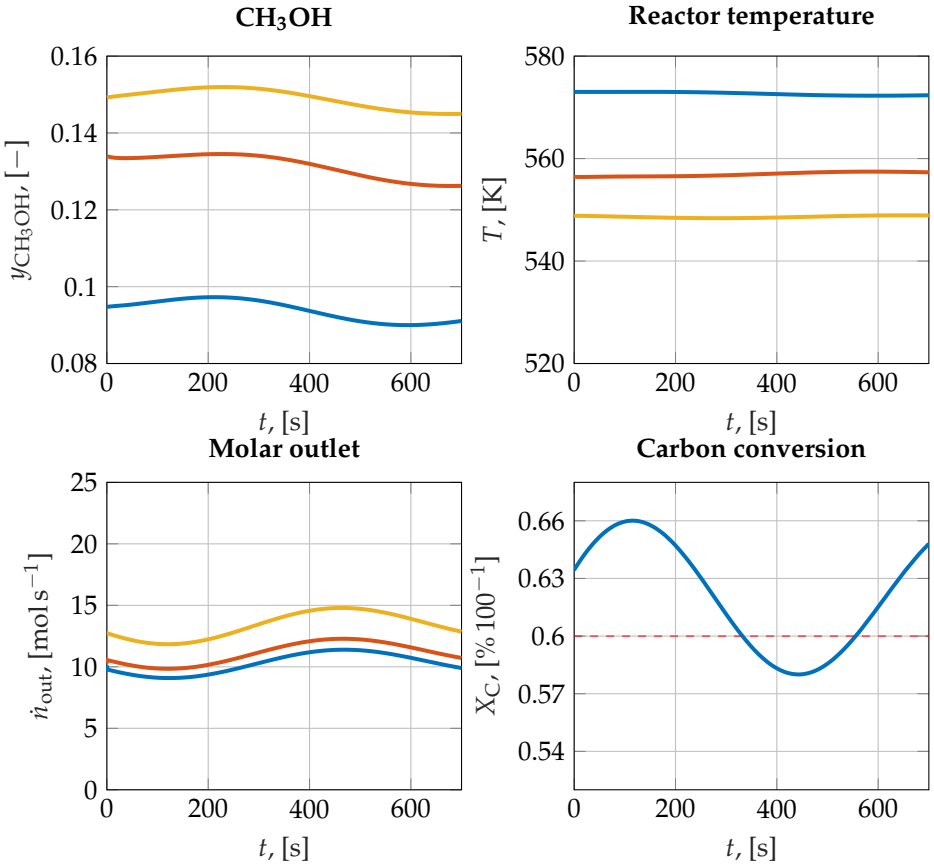

Figure 5. Simulation results for robust reactor design using $f_{\tilde{\xi}}$ as disturbance. Blue: first reactor, orange: second reactor, yellow: third reactor. The red dashed line in the lower right subplot indicates the required carbon conversion of 60%.

3.3. Dynamic Optimization

The dynamic optimization is the solution of Problem 3 (48).

The result for the robust design is shown in Figure 6, where the collocation support points are plotted.

The feed split ratios are chosen differently than for the robust steady-state design. The feed bypass to the third reactor is completely shut down, while the second reactor gets

more of the feed stream. For the first reactor, the value of the split is mostly close to that of the steady-state design, except for some drastic dynamic changes between 300 and 400 s, and 636 and 700 s. The first interval is located in the region where the simulation of the steady-state design became infeasible. Therefore, the optimizer has to choose a different control to achieve feasibility. The second interval comes due to the absence of terminal constraints, the objective function is increased by maximizing the output. In a practical application, the optimization would be repeated before this interval is reached.

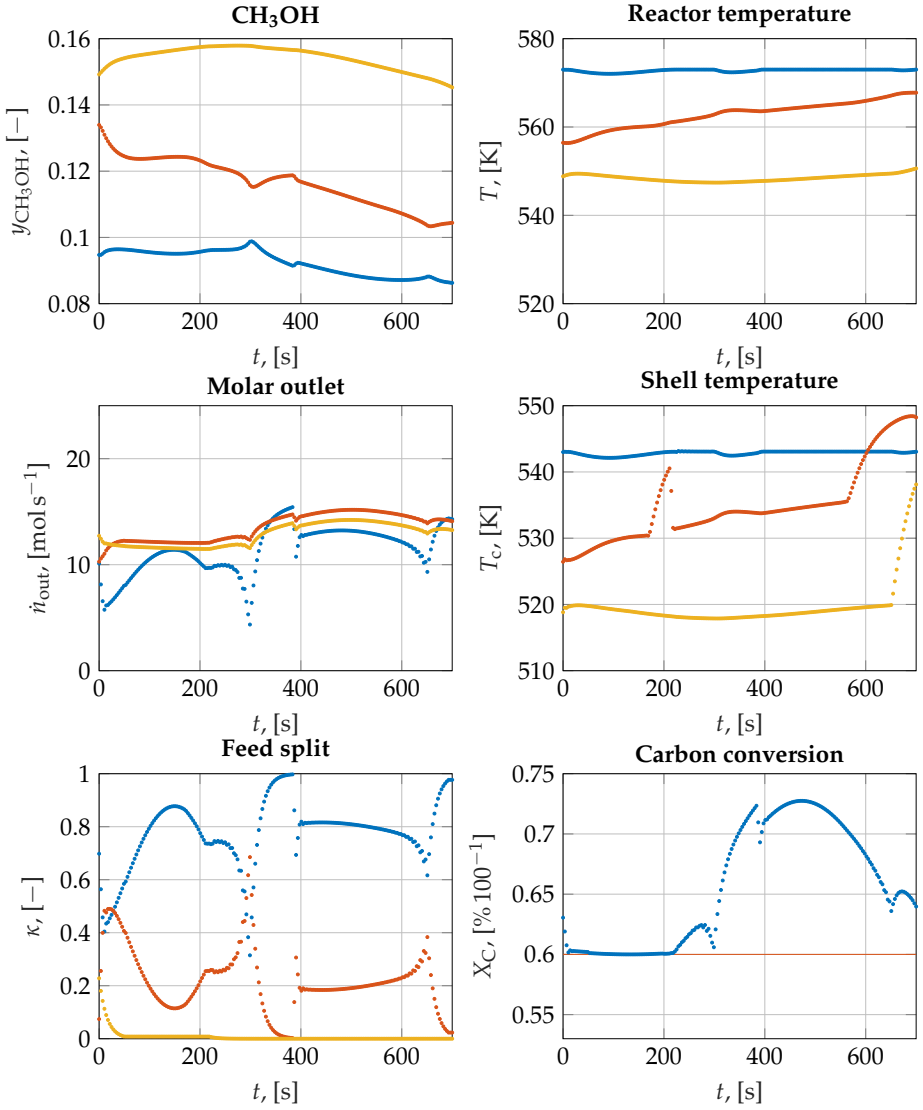

Figure 6. Results of the dynamic optimization using the values obtained from the robust reactor design for constant degrees of freedom, f_{ξ} is used as disturbance. Solution of Problem 3 (48). Blue: first reactor, orange: second reactor, yellow: third reactor. The red dashed line in the lower right subplot indicates the required carbon conversion of 60%.

The achieved space–time yield is $STY = 0.6987$, which is slightly below that of the robust case. It is, however, feasible.

The dynamic optimization for the nominal design converges to an infeasible point. The optimizer is not able to control the process such that the reactor temperatures remain within their bounds.

4. Conclusions

Methanol synthesis is a crucial topic in light of the upcoming changes in energy supply. As traditional steady-state processes will have to cope with energy fluctuations, they will also have to deal with fluctuations in their operating conditions. In this paper, we have investigated the influence of fluctuations on the inlet flow of a staged methanol synthesis reactor.

To address this challenge, both a nominal and a robust steady-state optimization of the reactor setup's operating conditions were conducted. As expected, the obtained optimal nominal reactor has a better performance than the robust reactor, which has to be more conservative in its design. However, for both designs, the dynamic behavior of the process was neglected, i.e., only steady-state optimizations were conducted. To take the transient behavior into account, both designs were tested with a predefined disturbance function. While the robust reactor is able to hold the imposed constraint on carbon conversion for a longer period, it ultimately also operates in an infeasible area.

In our case study, the disturbance is caused by fluctuating wind conditions. These wind conditions can be measured and predicted within a short time horizon. This provides an opportunity for a control scheme via dynamic optimization. To ensure feasible operation, an additional dynamic optimization was performed using fluctuation-specific split ratios and shell temperatures as degrees of freedom. While the nominal design converges to an infeasible point, the optimizer is able to control the operating conditions such that the robust reactor becomes feasible. Of course, the results depend on the imposed fluctuation function: its respective upper and lower bounds, as well as its dynamics. In a real application, additional buffer tanks would be used to make sure that the fluctuations exhibit desirable characteristics. Those tanks could also be included in the optimization problem to account for the buffer costs, which is, however, not the scope of this paper.

The approach presented in this paper can be interpreted as a feed-forward control scheme. In future works, we plan to enhance the dynamic optimization step used for calculating the control action with a machine learning-based approach [45]. For disturbances beyond the considered scenarios, an additional buffer tank for H_2 would be required. Simultaneous optimization of reactor and buffer designs under dynamic conditions is another interesting topic for future work. Furthermore, we intend to augment the overall control scheme with a feedback loop or, alternatively, conduct repetitive online optimizations to account for additional disturbances and plant model mismatch. The number of stages used in the present work was chosen exemplarily. Further work will be concerned with finding the optimal amount of stages for different scenarios. Additionally, the CSTRs will be replaced by industrially more relevant fixed bed reactor segments

In conclusion, this paper presents a novel approach to addressing the challenge of fluctuations in feed streams for methanol synthesis from renewable feedstock. By combining robust optimization with dynamic optimization, we have demonstrated that it is possible to generate a reactor design that is dynamically feasible for measurable fluctuating inlet conditions in a limited range.

Author Contributions: Conceptualization, T.K. and A.K.; methodology, T.K.; software, T.K.; validation, T.K.; formal analysis, T.K.; investigation, T.K.; resources, A.K.; data curation, T.K.; writing—original draft preparation, T.K.; writing—review and editing, T.K. and A.K.; visualization, T.K.; supervision, A.K.; project administration, A.K.; funding acquisition, A.K. All authors have read and agreed to the published version of the manuscript.

Funding: This work was funded by the German Research Foundation (DFG) within the priority program 2331 'Machine Learning in Chemical Engineering' under grant KI 417/9-1.

Data Availability Statement: Data are available upon request.

Conflicts of Interest: The funders had no role in the design of the study; in the collection, analyses, or interpretation of data; in the writing of the manuscript; or in the decision to publish the results.

Nomenclature

Symbols

r	$\mathrm{mol\,kg^{-1}\,s^{-1}}$	reaction rate
ϕ		catalyst state
k		rate constant
K		equilibrium constant
p_i	bar	partial pressure of component i
Θ^l		relative number of free surface centers
T	K	temperature
$\boldsymbol{\alpha}$		equilibrium constant parameters
A, B		reaction rate parameters
β		reaction kinetic parameter
y		mole fraction
γ		volume contraction
R	$\mathrm{J\,mol^{-1}\,K^{-1}}$	gas constant
ΔG	$\mathrm{J\,mol^{-1}}$	Gibbs free energy
n	mol	mole amount
m	kg	mass
$\nu_{i,j}$		stoichiometric coefficient of component i in reaction j
P	bar	pressure
$\mathrm{q_{sat}}$	$\mathrm{mol\,kg^{-1}}$	specific amount of surface centers
Θ_i		adsorption isotherms
V	$\mathrm{m^3}$	volume
h, h^*	$\mathrm{J\,mol^{-1}}$, $\mathrm{J\,kg^{-1}}$	enthalpy
$\dot{Q}$	$\mathrm{J\,s^{-1}}$	heat flow
Δh_R	$\mathrm{J\,kg^{-1}}$	heat of reaction
c_p	$\mathrm{J\,mol^{-1}\,K^{-1}}$	specific heat capacity
$\Delta \mathrm{h_{f,ref}}$	$\mathrm{J\,mol^{-1}}$	heat of formation
$\Delta \mathrm{h_{ads}}$	$\mathrm{J\,mol^{-1}}$	heat of adsorption
$\mathrm{K_W}$	$\mathrm{J\,m^{-2}\,K^{-1}\,s^{-1}}$	heat transfer coefficient
$\mathrm{A_W}$	$\mathrm{m^{-2}}$	cooling area
κ		feed split factor
ρ	$\mathrm{kg\,m^{-3}}$	density
ψ_C		CO, CO_2 split
STY	$\mathrm{mol\,m^{-3}\,s^{-1}}$	space time yield
J		objective function
ξ		disturbance
X_C		carbon conversion
x		degrees of freedom and optimization variables
U, s_1, s_2		punishment constant and slack variables

Subscripts

in	inlet
out	outlet
cat	catalyst
ref	reference
i, k	components [CH_3OH, CO_2, CO, H_2, H_2O]
j	reactions [CO-, CO_2-hydrogenation, WGS]
r	reactors [1, 2, 3]
tot	total
c	cooling
s	set-point

Superscripts

l	surface centers [(oxi), (red), (het)]
S	solid phase
G	gaseous phase
cat	catalyst

References

1. Olah, G.; Goeppert, A.; Prakash, K.S. *Beyond Oil and Gas: The Methanol Economy*, 2nd ed.; Wiley-VCH: Hoboken, NJ, USA, 2009.
2. Luyben, W.L. Design and Control of a Methanol Reactor/Column Process. *Ind. Eng. Chem. Res.* **2010**, *49*, 6150–6163. [CrossRef]
3. Räuchle, K.; Plass, L.; Wernicke, H.J.; Bertau, M. Methanol for Renewable Energy Storage and Utilization. *Energy Technol.* **2016**, *4*, 193–200. [CrossRef]
4. IRENA; Methanol Institute. *Innovation Outlook: Renewable Methanol*; Technical Report; International Renewable Energy Agency: Abu Dhabi, United Arab Emirates, 2021; ISBN 978-92-9260-320-5.
5. Zain, M.M.; Mohamed, A.R. An overview on conversion technologies to produce value added products from CH_4 and CO_2 as major biogas constituents. *Renew. Sustain. Energy Rev.* **2018**, *98*, 56–63. [CrossRef]
6. Zappa, W.; Junginger, M.; van den Broek, M. Is a 100% renewable European power system feasible by 2050? *Appl. Energy* **2019**, *233–234*, 1027–1050. [CrossRef]
7. Vita, A.; Vita, A.; Italiano, C.; Previtali, D.; Previtali, D.; Fabiano, C.; Palella, A.; Palella, A.; Freni, F.; Bozzano, G.; et al. Methanol synthesis from biogas: A thermodynamic analysis. *Renew. Energy* **2018**, *118*, 673–684. [CrossRef]
8. Theuerl, S.; Herrmann, C.; Heiermann, M.; Grundmann, P.; Landwehr, N.; Kreidenweis, U.; Kreidenweis, U.; Prochnow, A. The Future Agricultural Biogas Plant in Germany: A Vision. *Energies* **2019**, *12*, 396. [CrossRef]
9. Nestler, F.; Krüger, M.; Full, J.; Hadrich, M.J.; White, R.J.; Schaadt, A. Methanol Synthesis—Industrial Challenges within a Changing Raw Material Landscape. *Chem. Ing. Tech.* **2018**, *90*, 1409–1418. [CrossRef]
10. Bos, M.; Kersten, S.; Brilman, D. Wind power to methanol: Renewable methanol production using electricity, electrolysis of water and CO_2 air capture. *Appl. Energy* **2020**, *264*, 114672. [CrossRef]
11. Hoppe, W.; Bringezu, S.; Wachter, N. Economic assessment of CO_2-based methane, methanol and polyoxymethylene production. *J. CO2 Util.* **2018**, *27*, 170–178. [CrossRef]
12. Boudellal, M. *Power-to-Gas*; De Gruyter: Berlin, Germany, 2018. [CrossRef]
13. Sollai, S.; Porcu, A.; Tola, V.; Ferrara, F.; Pettinau, A. Renewable methanol production from green hydrogen and captured CO_2: A techno-economic assessment. *J. CO2 Util.* **2023**, *68*, 102345. [CrossRef]
14. Arnaiz del Pozo, C.; Cloete, S.; Ángel Jiménez, Á. Techno-economic assessment of long-term methanol production from natural gas and renewables. *Energy Convers. Manag.* **2022**, *266*, 115785. [CrossRef]
15. Stankiewicz, A.; Kuczynski, M. An industrial view on the dynamic operation of chemical converters. *Chem. Eng. Process. Process Intensif.* **1995**, *34*, 367–377. [CrossRef]
16. Kalz, K.F.; Kraehnert, R.; Dvoyashkin, M.; Dittmeyer, R.; Gläser, R.; Krewer, U.; Reuter, K.; Grunwaldt, J.D. Future Challenges in Heterogeneous Catalysis: Understanding Catalysts under Dynamic Reaction Conditions. *ChemCatChem* **2017**, *9*, 17–29. [CrossRef]
17. Mucci, S.; Mitsos, A.; Bongartz, D. Cost-Optimal Power-to-Methanol: Flexible Operation or Intermediate Storage? *arXiv* **2023**, arXiv:2305.18338.
18. Gabrel, V.; Murat, C.; Thiele, A. Recent advances in robust optimization: An overview. *Eur. J. Oper. Res.* **2014**, *235*, 471–483. [CrossRef]
19. Fischer, K.L.; Langer, M.R.; Freund, H. Dynamic Carbon Dioxide Methanation in a Wall-Cooled Fixed Bed Reactor: Comparative Evaluation of Reactor Models. *Ind. Eng. Chem. Res.* **2019**, *58*, 19406–19420. [CrossRef]
20. Fischer, K.L.; Freund, H. Intensification of load flexible fixed bed reactors by optimal design of staged reactor setups. *Chem. Eng. Process.* **2020**, *159*, 108183. [CrossRef]
21. Leyffer, S.; Menickelly, M.; Munson, T.; Vanaret, C.; Wild, S.M. A survey of nonlinear robust optimization. *INFOR Inf. Syst. Oper. Res.* **2020**, *58*, 342–373. [CrossRef]
22. Manenti, F.; Cieri, S.; Restelli, M.; Bozzano, G. Dynamic modeling of the methanol synthesis fixed-bed reactor. *Comput. Chem. Eng.* **2013**, *48*, 325–334. [CrossRef]
23. Haid, J.; Koss, U. Lurgi's Mega-Methanol technology opens the door for a new era in down-stream applications. In *Natural Gas Conversion VI*; Iglesia, E., Spivey, J., Fleisch, T., Eds.; Studies in Surface Science and Catalysis; Elsevier: Amsterdam, The Netherlands, 2001; Volume 136, pp. 399–404. [CrossRef]
24. Anicic, B.; Trop, P.; Goricanec, D. Comparison between two methods of methanol production from carbon dioxide. *Energy* **2014**, *77*, 279–289. [CrossRef]
25. Seidel, C.; Jörke, A.; Vollbrecht, B.; Seidel-Morgenstern, A.; Kienle, A. Kinetic modeling of methanol synthesis from renewable resources. *Chem. Eng. Sci.* **2018**, *175*, 130–138. [CrossRef]
26. Seidel, C.; Jörke, A.; Vollbrecht, B.; Seidel-Morgenstern, A.; Kienle, A. Corrigendum to "Kinetic modeling of methanol synthesis from renewable resources" (Chem. Eng. Sci. 175 (2018) 130–138). *Chem. Eng. Sci.* **2020**, *223*, 115724. [CrossRef]
27. Seidel, C.; Nikolic, D.; Felischak, M.; Petkovska, M.; Seidel-Morgenstern, A.; Kienle, A. Optimization of Methanol Synthesis under Forced Periodic Operation. *Processes* **2021**, *9*, 872. [CrossRef]
28. Graaf, G.; Sijtsema, P.; Stamhuis, E.; Joosten, G. Chemical equilibria in methanol synthesis. *Chem. Eng. Sci.* **1986**, *41*, 2883–2890. [CrossRef]
29. Graaf, G.; Stamhuis, E.; Beenackers, A. Kinetics of low-pressure methanol synthesis. *Chem. Eng. Sci.* **1988**, *43*, 3185–3195. [CrossRef]
30. Bussche, K.; Froment, G. A Steady-State Kinetic Model for Methanol Synthesis and the Water Gas Shift Reaction on a Commercial $Cu/ZnO/Al_2O_3$ Catalyst. *J. Catal.* **1996**, *161*, 1–10. [CrossRef]

31. Nikolić, D.; Seidel, C.; Felischak, M.; Miličić, T.; Kienle, A.; Seidel-Morgenstern, A.; Petkovska, M. Forced periodic operations of a chemical reactor for methanol synthesis—The search for the best scenario based on Nonlinear Frequency Response Method. Part I Single input modulations. *Chem. Eng. Sci.* **2022**, *248*, 117134. [CrossRef]
32. Reid, R.C.; Prausnitz, J.M.; Poling, B.E. *The Properties of Gases and Liquids*; McGraw-Hill Professional: New York, NY, USA, 1987.
33. Torcida, M.F.; Curto, D.; Martín, M. Design and optimization of CO2 hydrogenation multibed reactors. *Chem. Eng. Res. Des.* **2022**, *181*, 89–100. [CrossRef]
34. Johnson, M.; Heggs, P.J.; Mahmud, T. Assessment of Overall Heat Transfer Coefficient Models to Predict the Performance of Laboratory-Scale Jacketed Batch Reactors. *Org. Process. Res. Dev.* **2016**, *20*, 204–214. [CrossRef]
35. Roetzel, W.; Spang, B. C2 Wärmeübertrager: Wärmedurchgang und Wärmedurchgangskoeffizienten. In *VDI-Wärmeatlas: Fachlicher Träger VDI-Gesellschaft Verfahrenstechnik und Chemieingenieurwesen*; Stephan, P., Kabelac, S., Kind, M., Mewes, D., Schaber, K., Wetzel, T., Eds.; Springer: Berlin/Heidelberg, Germany, 2019; pp. 79–97. [CrossRef]
36. Fischer, K.L.; Freund, H. On the optimal design of load flexible fixed bed reactors: Integration of dynamics into the design problem. *Chem. Eng. J.* **2020**, *393*, 124722. [CrossRef]
37. Bezanson, J.; Edelman, A.; Karpinski, S.; Shah, V.B. Julia: A fresh approach to numerical computing. *SIAM Rev.* **2017**, *59*, 65–98. [CrossRef]
38. Lubin, M.; Dowson, O.; Garcia, J.D.; Huchette, J.; Legat, B.; Vielma, J.P. JuMP 1.0: Recent improvements to a modeling language for mathematical optimization. *Math. Program. Comput.* **2023**, *15*, 581–589. [CrossRef]
39. Pulsipher, J.L.; Zhang, W.; Hongisto, T.J.; Zavala, V.M. A Unifying Modeling Abstraction for Infinite-Dimensional Optimization. *Comput. Chem. Eng.* **2021**, *156*, 107567. [CrossRef]
40. Kelly, M. An Introduction to Trajectory Optimization: How to Do Your Own Direct Collocation. *SIAM Rev.* **2017**, *59*, 849–904. [CrossRef]
41. Byrd, R.H.; Nocedal, J.; Waltz, R.A. Knitro: An Integrated Package for Nonlinear Optimization. In *Large-Scale Nonlinear Optimization*; Di Pillo, G., Roma, M., Eds.; Springer: Boston, MA, USA, 2006; pp. 35–59. [CrossRef]
42. Fraunhofer ISE. Energy-Charts. Available online: https://www.energy-charts.info/ (accessed on 19 May 2023).
43. Bundesnetzagentur. SMARD Strommarktdaten. Available online: https://www.smard.de/ (accessed on 6 July 2023).
44. Rackauckas, C.; Nie, Q. DifferentialEquations.jl—A Performant and Feature-Rich Ecosystem for Solving Differential Equations in Julia. *J. Open Res. Softw.* **2017**, *5*, 15. [CrossRef]
45. Martensen, C.J.; Plate, C.; Keßler, T.; Kunde, C.; Kaps, L.; Kienle, A.; Seidel-Morgenstern, A.; Sager, S. Towards Machine Learning for Power2X Processes. *Comput. Aided Chem. Eng.* **2023**, *52*, 561–568. [CrossRef]